Supplementary Information

An Essential Descriptor for Oxygen Evolution Reaction on Reducible Metal Oxide Surfaces

Xiang Huang,‡[a,b] Jiong Wang,‡[c] Hua Bing Tao,‡[c] Hao Tian,[a] and Hu Xu*[a]

a Department of Physics, Southern University of Science and Technology, Shenzhen 518055, China

b School of Physics and Technology, Wuhan University, Wuhan 430072, China

c School of Chemical and Biomedical Engineering, Nanyang Technological University, 62 Nanyang Drive, Singapore 637459, Singapore

* To whom correspondence should be addressed. Email: xuh@sustc.edu.cn

‡ X.H., J.W., and H.T. contributed equally to this work.

Methods

1. Calculation details

Spin-polarized density functional theory (DFT) calculations are performed using generalized gradient approximation (GGA) in the form of revised Perdew-Burke-Ernzerhof (RPBE) for the exchange-correlation potentials,[1-3] the projector augmented wave method,[4] and a plane-wave basis set of 450 eV, as implemented in the Vienna ab initio simulation package (VASP).[5, 6] The convergence criteria for electronic and ionic iterations are set as 10^{-4} eV and 0.02 eV/Å, respectively. Dipole corrections are taken into account throughout the calculations.

The oxygen evolution reactions (OER) are carried out on the surfaces of several typical reducible metal oxides including TiO_2, SnO_2, NiO, WO_3, and ZnO, which are of rutile, rutile, rock salt, γ-monoclinic, and wurtzite phases, respectively. The TiO_2(110), TiO_2(100), TiO_2(101), SnO_2(110), NiO(001), ZnO($10\bar{1}0$), and WO_3(001) surfaces are simulated using slab models composed of (4×1), (1×4), (2×1), (4×1), ($2\sqrt{2} \times 2\sqrt{2}$), (4×2) and (2×2) supercells with fifteen, fifteen, fifteen, fifteen, four, eight, and nine atomic monolayers, respectively. The vacuum layers are set to ~13 Å to decouple the interaction between neighboring images. The surface Brillouin-zones are sampled with Gamma centered k-grids of 2×4×1, 6×2×1, 2×6×1, 2×4×1, 4×4×1, 2×2×1, and 4×4×1, respectively. During optimization, the bottom three atomic monolayers for TiO_2(110), TiO_2(100), TiO_2(101) and SnO_2(110), and two atomic monolayers for NiO(001) and ZnO($10\bar{1}0$) are fixed at their bulk positions while the rest atomic layers and adsorbates are free to move in all directions. For WO_3(001) surface, we transfer half of the oxygen atoms from the top to the bottom layer, in order to eliminate the dipole perpendicular to the surface.[7, 8] All of the atoms in WO_3(001) slab and adsorbates are freely relaxed during optimization. The energies of gas-phase H_2 and H_2O are calculated in a box in the size of 20×20×20 Å with Gamma point. For the calculations of OER on V, Nb, Ta, Mo, and W atoms doped TiO_2(110), a (2×1) supercell is adopted. The OER takes place on a five-fold coordinated Ti atom (Ti^{5c}) on the TiO_2(110) surface, corresponding to *OH, *O, and *OOH at coverage of

0.5 ML, which is considered as the "standard" coverage in the reaction.[9] K-mesh of 4×4×1 is used to sample the surface Brillouin-zone. The other setups are identical to those of TiO_2(110)-p(4×1) supercell. For NiO and WO_3, we apply the Hubbard-U corrections to the d-electrons of Ni and W following the approach proposed by Dudarev et al.[10] The values of the effective Hubbard-U parameter, U=6.45 eV and 6.2 eV are chosen for Ni and W, respectively.[11, 12]

2. Free energy diagram

We consider the OER following the four-electron mechanism, which comprises four reaction steps, shown as below

$$H_2O_{(l)} \rightarrow OH^* + H^+ + e^- \quad (1)$$

$$OH^* \rightarrow O^* + H^+ + e^- \quad (2)$$

$$O^* + H_2O_{(l)} \rightarrow OOH^* + H^+ + e^- \quad (3)$$

$$OOH^* \rightarrow * + O_{2(g)} + H^+ + e^- \quad (4)$$

The asterisk (*) represents the active site on the surfaces of catalysts, and *OH, *O, and *OOH denote the adsorbed *OH, *O, and *OOH, respectively.

The free energies of the reactants, products, and reaction intermediates are defined as

$$G = E_{DFT} + E_{ZPE} - TS$$

where E_{DFT} represents the electronic energy calculated by DFT, E_{ZPE} represents zero point energy estimated within the harmonic approximation, and TS represents entropy at 298.15 K. For the gas-phase molecule, the entropy is obtained directly from the standard thermodynamic database.[13] The E_{ZPE} and TS of gas-phase molecules and reaction intermediates are listed in Table S1. The vibrational frequencies of intermediates are listed in Table S2. For the reaction step containing the transfer of proton and electron, the free energy of a pair of proton and electron ($H^+ + e^-$) can be calculated as a function of applied potential relative to reversible hydrogen

electrode (U *vs* RHE), i.e., $\mu(H^+) + \mu(e^-) = \frac{1}{2}\mu(H_2) - eU$, according to the computational hydrogen electrode (CHE) model proposed by Nørskov.[14] The potential determining step (pds) is defined as the highest free energy step in the four-step mechanism, and therefore it is the last step to become downhill in free energy with the increase of potential. We use the energies of H_2O and H_2 molecules calculated by DFT together with experimental formation energy of H_2O (4.92 eV) to construct the free energy diagram. The free energies of O_2, *OOH, *O, and *OH at a given potential U relative to RHE are defined as

$$\Delta G(O_2) = 4.92 - 4eU$$

$$\Delta G(OOH) = G(OOH^*) + \frac{3G(H_2)}{2} - G(*) - 2G(H_2O) - 3eU$$

$$\Delta G(O) = G(O^*) + G(H_2) - G(*) - G(H_2O) - 2eU$$

$$\Delta G(OH) = G(OH^*) + \frac{G(H_2)}{2} - G(*) - G(H_2O) - eU$$

3. The approach of bringing in excess electrons

To tune NEE from 0 to 2 *e*, we choose one bridge O atom (two adjacent bridge O atoms) on the TiO_2(110) surface to adsorb one H atom (two H atoms) with different charges, which are available in VASP pseudopotential library. Considering the fact that each O vacancy generates two excess electrons in TiO_2(110),[15-19] it is reasonable that one chemisorbed H atom can bring in excess electrons in the same quantity of its valance electrons.[20-22] Besides, we investigate the effect of different combinations and different adsorption sites of H atoms on the binding energies of *OH, *O, and *OOH, as listed in Table S3.

Table S1. Zero point energy (ZPE) and entropy corrections used to calculate free energies of reactants, products, and reaction intermediates. The ZPE is calculated using a p(2×1) supercell with *OH, *O, and *OOH at coverage of 0.5 ML. The gas phase H_2O at 0.035 atm is taken as reference because at this pressure gas H_2O is in equilibrium with liquid H_2O.

	ZPE (eV)	TS (eV) (T=298.15K)	ΔG_{corr} (eV)
H_2O	0.570	0.670	-0.100
H_2	0.270	0.400	-0.130
*OH	0.335	0	0.335
*O	0.063	0	0.063
*OOH	0.431	0	0.431

Table S2. Harmonic vibrational frequencies for *OH, *O, and *OOH on TiO_2(110).

Species	Frequencies (cm^{-1})
*OH	3748.7, 623.9, 517.6, 206.0, 169.8, 143.4
*O	675.8, 168.4, 167.6
*OOH	3617.6, 1343.4, 921.1, 384.2, 216.4, 191.8, 116.2, 82.3, 77.2

Table S3. The charges (unit in *e*) of hydrogen atoms chosen to chemisorb on bridge O (O^{2c}) atoms on TiO_2(110) to introduce excess electrons, as well as the corresponding binding energies (unit in eV) of OCI, potential determining step (pds), and overpotentials (unit in V) on the resultant surfaces. Numbers of 1 and 2 in circle denote the position of O atoms, as shown in Figure S1.

Charge (*e*)								
①O^{2c}	②O^{2c}	Total charge	ΔG_{OH}	ΔG_{O}	ΔG_{OOH}	ΔG_{OOH}-ΔG_{OH}	pds	Overpotential
0.5	0.5	1	0.16	2.06	3.72	3.56	*OH→*O	0.67
0.58	0.42	1	0.15	2.04	3.72	3.57	*OH→*O	0.66
0.5	0.58	1.08	0.15	1.92	3.71	3.56	*O→*OOH	0.56
0.58	0.5	1.08	0.14	1.90	3.70	3.56	*O→*OOH	0.57
0.5	0.66	1.16	0.14	1.78	3.68	3.54	*O→*OOH	0.67
0.66	0.5	1.16	0.13	1.76	3.67	3.55	*O→*OOH	0.69

Table S4. Binding energies (eV) of *OH (ΔG_{OH}),*OOH (ΔG_{OOH}), and their difference (ΔG_{OOH}–ΔG_{OH}) calculated at coverage of 0.5 ML, 0.33 ML, 0.25 ML, 0.167 ML and 0.125 ML, respectively, on the perfect TiO_2(110) surface.

Coverage	0.5 ML	0.33 ML	0.25 ML	0.167 ML	0.125 ML
k-mesh	4×4×1	3×4×1	2×4×1	3×2×1	2×2×1
ΔG_{OH}	1.68	1.58	1.34	1.34	0.99
ΔG_{OOH}	4.97	4.97	4.86	4.86	4.53
ΔG_{OOH}–ΔG_{OH}	3.29	3.39	3.52	3.52	3.54

Table S5. Binding energies (unit in eV) of *OH, *O, and *OOH on one V, Nb, Ta, Mo, or W atom doped TiO_2(110), with the corresponding potential determining step (pds) and overpotentials (unit in V). (b), (d), (e), and (f) denote the configurations shown in Figure 4.

configuration	elements	ΔG_{OH}	ΔG_{O}	ΔG_{OOH}	pds	overpotential
(b)	V	0.093	2.226	3.642	*OH→*O	0.902
	Nb	0.117	2.187	3.659	*OH→*O	0.839
	Ta	0.050	2.115	3.605	*OH→*O	0.835
	Mo	0.131	0.411	3.614	*O→*OOH	1.973
	W	0.098	0.244	3.587	*O→*OOH	2.113
(d)	Mo	0.302	1.487	3.821	*O→*OOH	1.104
	W	-0.087	0.839	3.444	*O→*OOH	1.375
(e)	Mo	0.308	1.956	3.850	*O→*OOH	0.663
	W	0.080	1.341	3.620	*O→*OOH	1.049
(f)	Mo	0.465	2.239	4.002	*OH→*O	0.545
	W	0.267	1.789	3.803	*O→*OOH	0.784

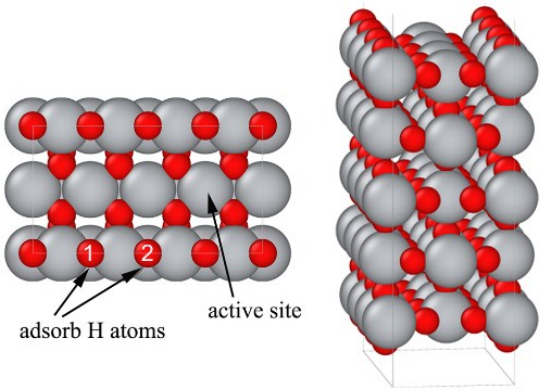

Figure S1. Top and side views of TiO_2(110) slab model used in the calculation. Two bridge O atoms (O^{2c}) labeled in 1 and 2 are chosen to adsorb H atoms with different charges to tune the number of excess electrons in TiO_2. The Ti^{5c} atom is the active site for the oxygen evolution reaction. The Ti and O atoms are marked by gray and red spheres, respectively.

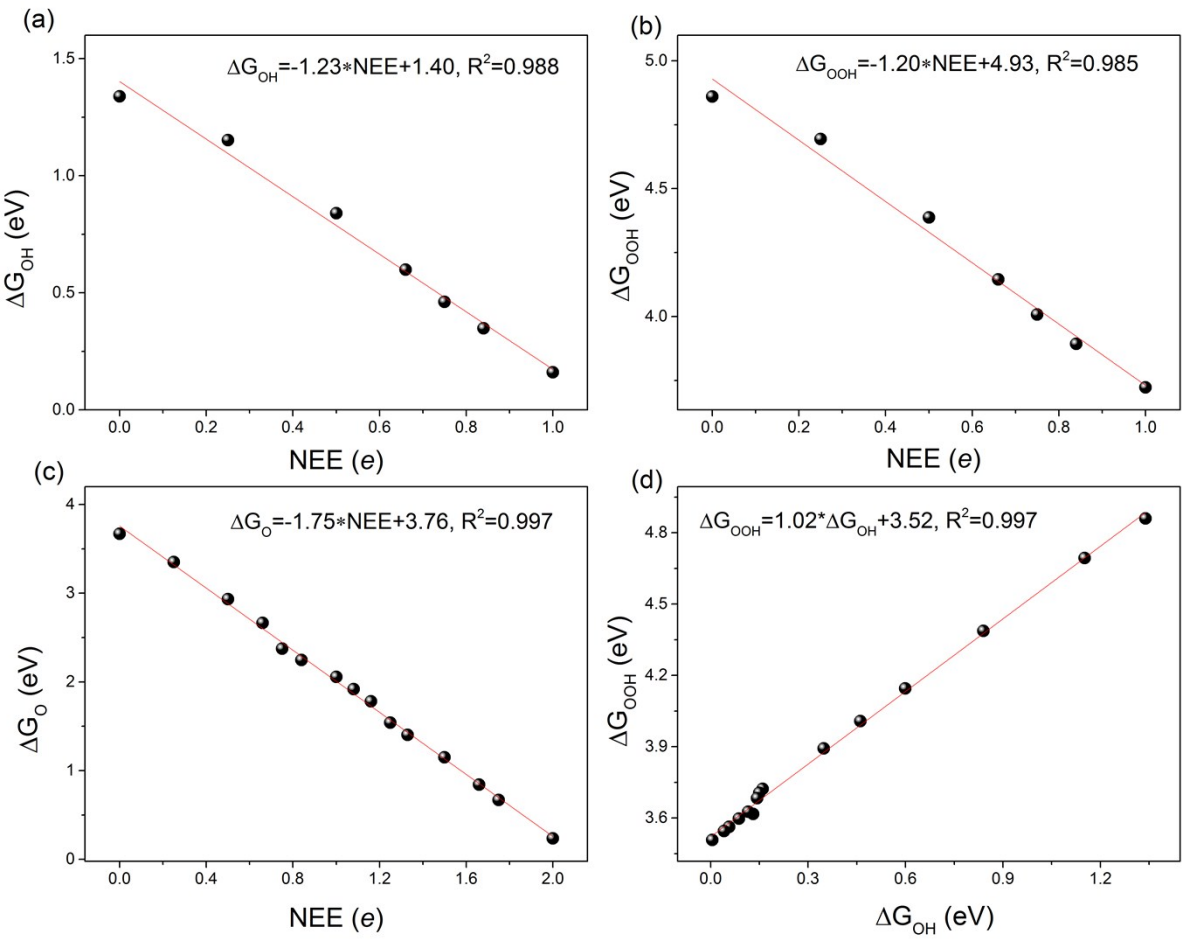

Figure S2. Scaling relations of binding energies of (a) *OH, (b) *OOH, and (c) *O with NEE. (d) Scaling relation between binding energies of *OOH and *OH.

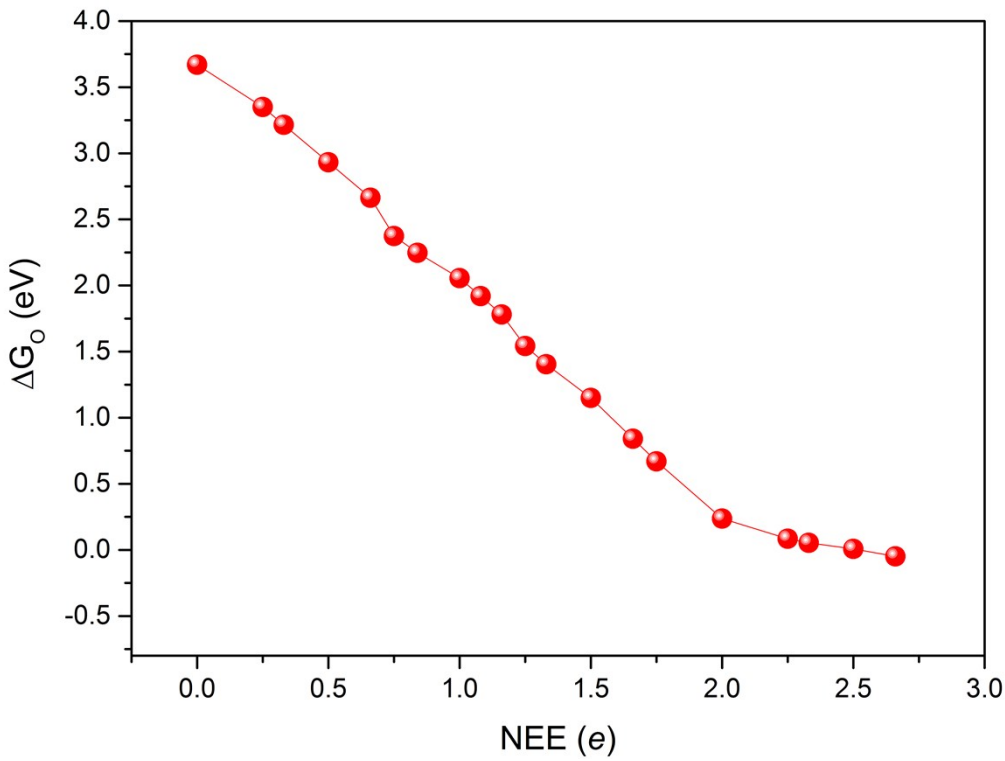

Figure S3. Binding energy of *O plotted as a function of NEE. An inflection point appears at NEE=2 *e*.

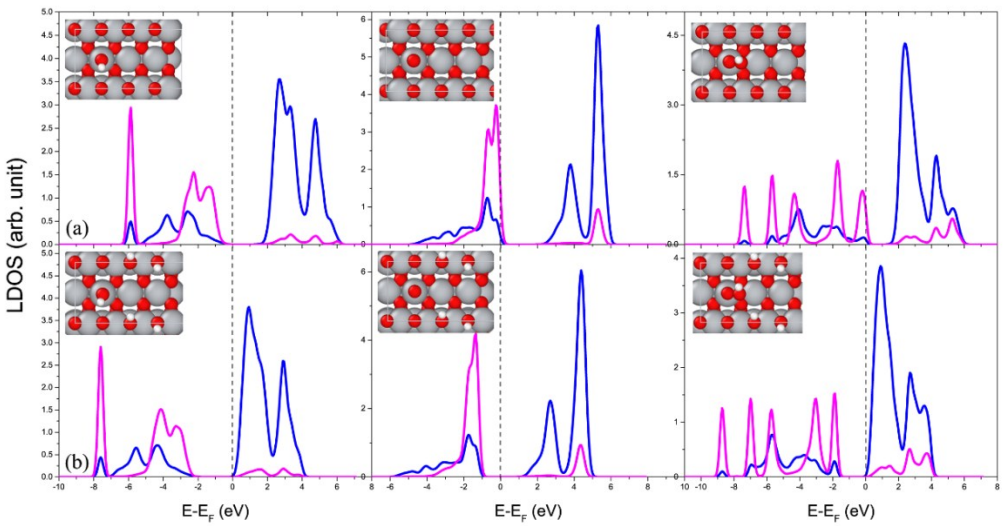

Figure S4. LDOS for *p* orbitals of O atoms in *OH, *O, and *OOH (purple), and *d* orbitals of bonded Ti^{5c} atom (blue) at NEE of (a) 0 and (b) 2 *e*, respectively. The hybridization peaks in the case of NEE=2 *e* are obviously down shifted with respect to those at NEE=0, indicating that the bonding of *OH, *O, and *OOH with Ti^{5c} atom are enhanced. The Ti, O, and H atoms are marked by gray, red, and white spheres, respectively.

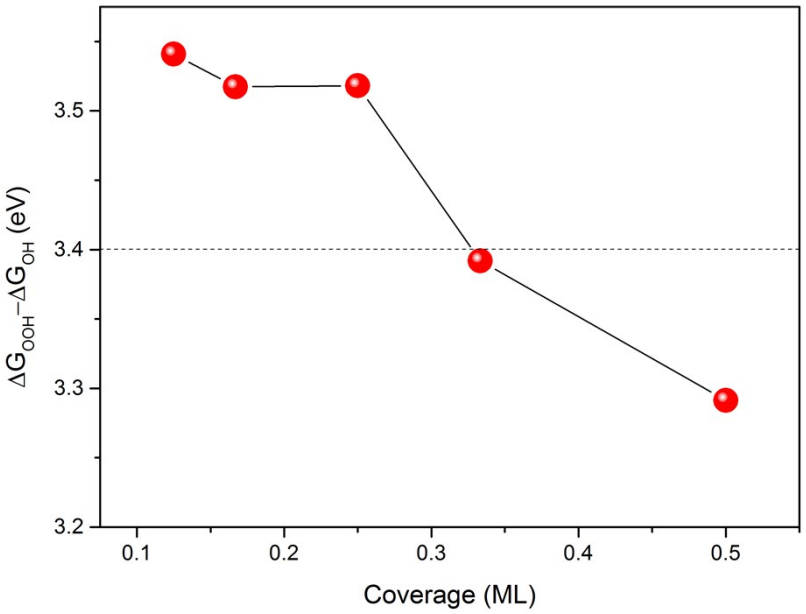

Figure S5. Variation of $\Delta G_{OOH}-\Delta G_{OH}$ with the change of coverage. The dash line indicates the upper boundary of the scaling relation of $\Delta G_{OOH}-\Delta G_{OH} = 3.2 \pm 0.2$ eV.

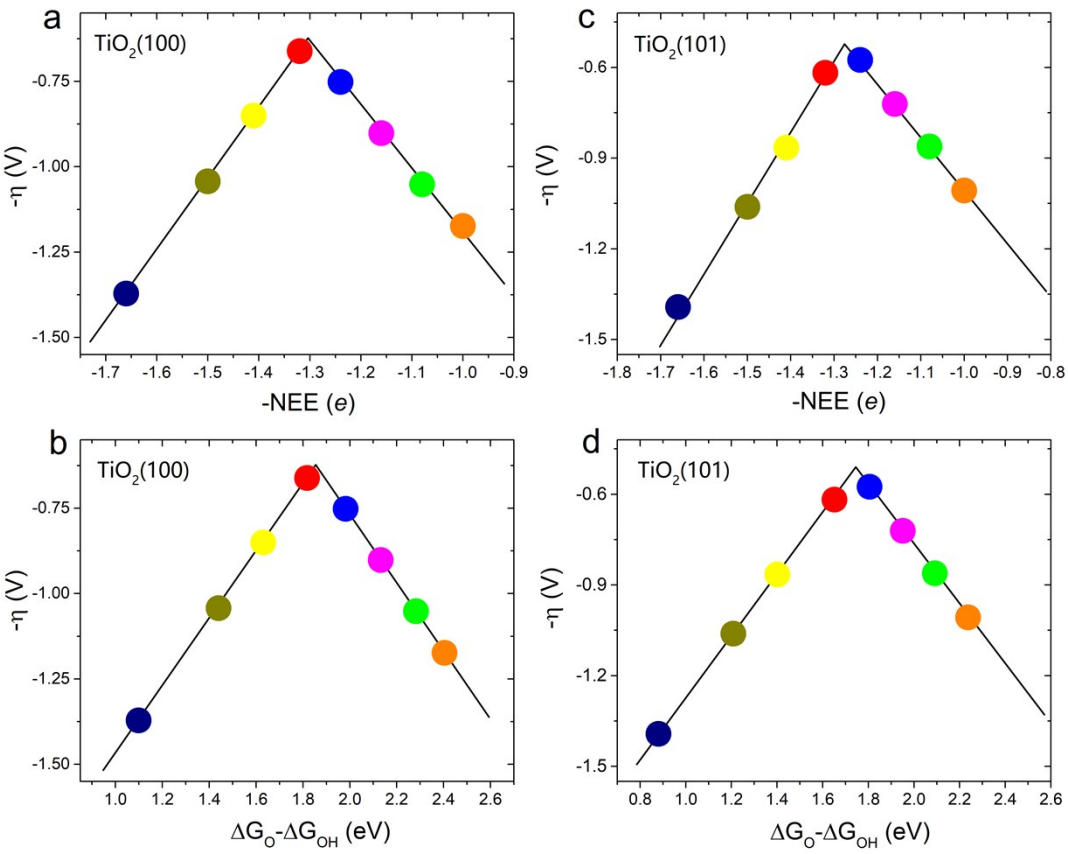

Figure S6. OER activities of the $TiO_2(100)$ and $TiO_2(101)$ surfaces plotted as the function of negative NEE (–NEE) and ΔG_O-ΔG_{OH}. The points in (a) and (b) with the same color denote the same set of data. The same applies to (c) and (d).

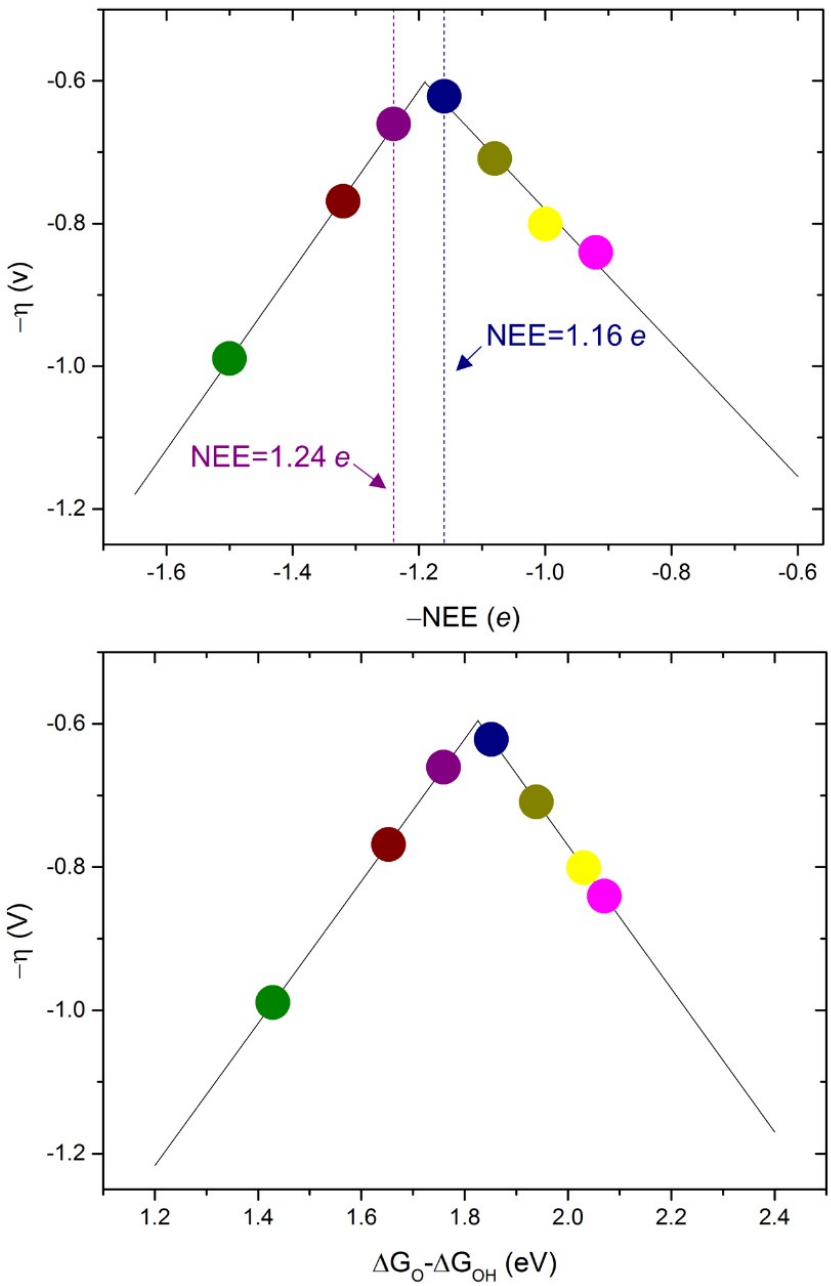

Figure S7. OER activity of WO_3(001) surface plotted as the function of (a) (–NEE) and (b) $\Delta G_O – \Delta G_{OH}$. The points in (a) and (b) with the same color denote the same set of data.

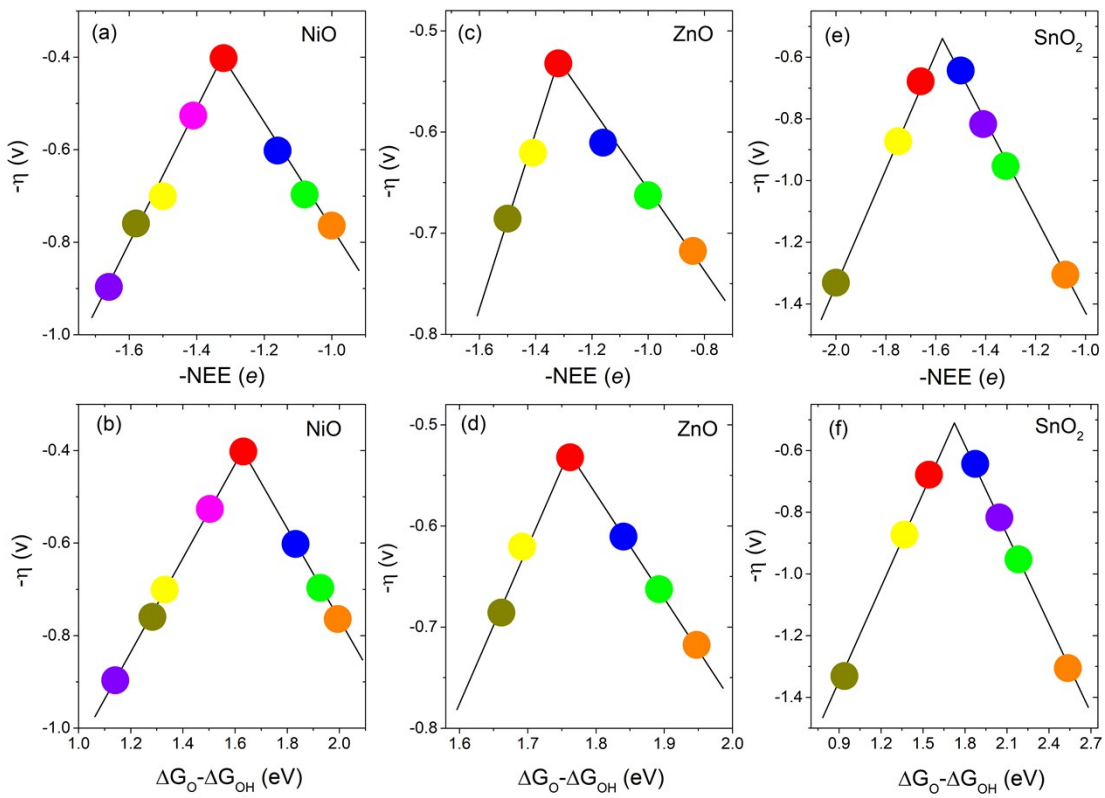

Figure S8. OER activities of the NiO(001), ZnO($10\bar{1}0$), and SnO_2(110) surfaces plotted as the function of negative NEE (–NEE) and ΔG_O-ΔG_{OH}. The points in (a) and (b) with the same color denote the same set of data. The same applies to (c)-(d) and (e)-(f).

References

1 J. P. Perdew, M. Ernzerhof and K. Burke, *J. Chem. Phys.*, 1996, **105**, 9982-9985.

2 J. P. Perdew, K. Burke and M. Ernzerhof, *Phys. Rev. Lett.*, 1996, **77**, 3865-3868.

3 B. Hammer, L. B. Hansen and J. K. Nørskov, *Phys. Rev. B*, 1999, **59**, 7413-7421.

4 G. Kresse and D. Joubert, *Phys. Rev. B*, 1999, **59**, 1758-1775.

5 G. Kresse and J. Furthmüller, *Phys. Rev. B*, 1996, **54**, 11169-11186.

6 G. Kresse and J. Furthmüller, *Comp. Mater. Sci.*, 1996, **6**, 15-50.

7 H. Jin, J. Zhu, J. Hu, Y. Li, Y. Zhang, X. Huang, K. Ding and W. Chen, *Theor. Chem. Acc.*, 2011, **130**, 103.

8 F. Wang, C. Di Valentin and G. Pacchioni, *J. Phys. Chem. C*, 2012, **116**, 10672-10679.

9 M. García-Mota, A. Vojvodic, H. Metiu, I. C. Man, H.-Y. Su, J. Rossmeisl and J. K. Nørskov, *ChemCatChem*, 2011, **3**, 1607-1611.

10 S. L. Dudarev, G. A. Botton, S. Y. Savrasov, C. J. Humphreys and A. P. Sutton, *Phys. Rev. B*, 1998, **57**, 1505-1509.

11 W. Zhao, A. D. Doyle, S. E. Morgan, M. Bajdich, J. K. Nørskov and C. T. Campbell, *J. Phys. Chem. C*, 2017, **121**, 28001-28006.

12 M. García-Mota, A. Vojvodic, F. Abild-Pedersen and J. K. Nørskov, *J. Phys. Chem. C*, 2013, **117**, 460-465.

13 C. J. Cramer, 2004.

14 J. K. Nørskov, J. Rossmeisl, A. Logadottir, L. Lindqvist, J. R. Kitchin, T. Bligaard and H. Jonsson, *J. Phys. Chem. B*, 2004, **108**, 17886-17892.

15 Y.-Y. Yu and X.-Q. Gong, *ACS Catal.*, 2015, **5**, 2042-2050.

16 H. Tian, B. Xu, J. Fan and H. Xu, *J. Phys. Chem. C*, 2018, **122**, 8270-8276.

17 P. Deák, B. Aradi and T. Frauenheim, *Phys. Rev. B*, 2015, **92**, 045204.

18 C. M. Yim, C. L. Pang and G. Thornton, *Phys. Rev. Lett.*, 2010, **104**, 036806.

19 Z. Helali, A. Jedidi, O. A. Syzgantseva, M. Calatayud and C. Minot, *Theor. Chem. Acc.*, 2017, **136**, 100.

20 C. Di Valentin, G. Pacchioni and A. Selloni, *Phys. Rev. Lett.*, 2006, **97**, 166803.

21 Z.-T. Wang, J. C. Garcia, N. A. Deskins and I. Lyubinetsky, *Phys. Rev. B*, 2015, **92**, 081402.

22 N. A. Deskins, R. Rousseau and M. Dupuis, *J. Phys. Chem. C*, 2009, **113**, 14583-14586.